Probable heat capacity signature of the supersolid transition

X. Lin[1], A. C. Clark[1] & M. H. W. Chan[1]

Liquid ^{4}He enters the superfluid state and flows without friction below 2.176 K. Thin liquid films adsorbed on solid substrates undergo the same transformation, although at a lower temperature. When the substrate is subjected to oscillatory motion a portion of the film, known as the superfluid fraction, decouples from the oscillation. A similar phenomenon has been observed[1,2] in solid ^{4}He, in which a fraction of the solid seems to decouple from the motion of the surrounding lattice. Although this observation has been replicated in various laboratories[3-6], no thermodynamic signature of the possible supersolid transition has been seen. Here we report the finding of a heat capacity peak that coincides with the onset of mass decoupling. This complementary experimental evidence supports the existence of a genuine transition between the normal solid and supersolid phases of ^{4}He.

The superfluid-like behaviour—that is, nonclassical rotational inertia[7] (NCRI)—of solid ^{4}He appears as a decrease in the period of a sample cell under torsional motion. Relative to the total amount of ^{4}He in the torsion cell, the NCRI fraction (NCRIF) ranges[8] from 0.03% to as high as 20%. The variation suggests that crystalline defects within the solid greatly influence the phenomenon[3,9,10]. Most of the samples studied so far were grown with commercial high-purity ^{4}He gas (~0.3 p.p.m. ^{3}He) by the blocked-capillary method[10]. The temperature dependence of NCRIF, characterized by saturation at low temperature and a gradual decay to zero at high temperature, is qualitatively reproduced in all measurements[1-6,8,10]. The onset temperature T_o, the point at which NCRI becomes resolvable from the noise, varies between 160 and 400 mK. In samples diluted with higher concentrations of ^{3}He, T_o is found to extend to even higher temperature, both in confined geometries[1] and in the bulk (E. Kim, J. S. Xia, J. T. West, X.L. and M.H.W.C., unpublished observations). A recent model equates NCRI to the rotational susceptibility of a vortex liquid phase[11]. According to this model, the high-temperature tail of NCRI reflects the finite response time of vortices to the oscillating flow fields generated by the torsional oscillator. The coupling of ^{3}He atoms to the cores of such vortices will further slow their response, because they must be dragged through the lattice. The consequence of this interaction is to extend the apparent onset to higher temperature, as observed. In addition, it was found[10] that for solid ^{4}He containing ~1 p.p.b. ^{3}He the NCRIF data of eight different samples collapse onto a single curve with a distinctly sharper onset temperature, $T_o = 75 \pm 5$ mK (mean $\pm$ s.d). Last, a frequency effect[6] consistent with this theoretical model has also been observed.

If the observed NCRI is the signature of a genuine second-order phase transition, there should be a peak in heat capacity at the transition. Many measurements[12-17] of the heat capacity of solid ^{4}He have been made since the 1960s, all reporting the T^3 dependence expected for a Debye solid at low temperature. However, the resolution of these experiments below 100 mK is severely limited by the heat

capacity of the sample cells, which is typically more than 20-fold that of solid ^{4}He. (See Supplementary Discussion for further experimental details.)

Our sample cell consists of undoped silicon, a small aluminium cap and a minimal amount of epoxy (see inset to Fig. 1). The virtue of silicon is its small heat capacity and high thermal conductivity at low temperature. The aluminium cap is necessary to create a reliable seal between the capillary and silicon. The cell is filled through a thin glass capillary with an inner diameter of 0.1 mm, and is mechanically secured to the refrigerator with nylon screws. Measurements were made with an alternating-current method[18], where the frequency of the applied power is low enough to maintain thermal equilibrium between the entire sample cell and solid helium, but high enough for the alternating-current modulation not to be 'lost' through the weak thermal link (a copper wire 5 cm in length and 0.08 mm in diameter) to the mixing chamber. These conditions were satisfied between 0.05 and 0.5 Hz. The data presented here were obtained at 0.1 Hz.

Solid samples were grown by using the blocked capillary method. In addition to forming samples from ^{4}He gas containing 1 p.p.b. or 0.3 p.p.m. ^{3}He, dilute solid mixtures were grown with ^{3}He
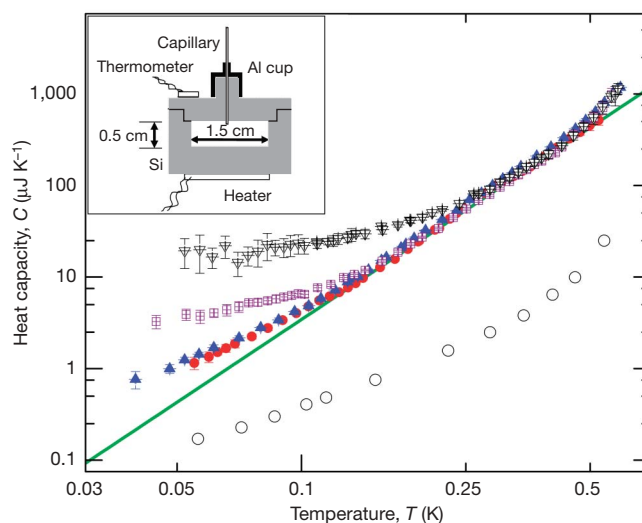

Figure 1 | Heat capacity of four samples containing different amounts of ^{3}He impurities. The green line is the expected T^3 dependence for a Debye solid. The error bar at each T is determined by the s.d. of 10–20 successive measurements, and is typically 2% of C. The measured temperature oscillation scales inversely with the heat capacity; the scatter at low temperature is the largest for the 30 p.p.m. sample. Black open triangles, 30 p.p.m.; purple open squares, 10 p.p.m.; blue triangles, 0.3 p.p.m.; red circles, 1 p.p.b. The empty-cell background, which has been subtracted, is also shown (black open circles). Inset, diagram of the silicon cell, with an internal volume of 0.926 cm^3.

[1]Department of Physics, The Pennsylvania State University, University Park, Pennsylvania 16802, USA.

concentrations of $x_3 = 10$ p.p.m. and 30 p.p.m. These samples were prepared by condensing a small, measured quantity of ^{3}He into the cell before the introduction of commercially pure ^{4}He. The uncertainties in x_3 of the 10 p.p.m. and 30 p.p.m. samples are estimated to be 30% and 20%, respectively. (See Supplementary Discussion for further information on ^{3}He impurities.) The limited accuracy stems from the extra volume ($2\,cm^3$) with a large surface area that is connected to the sample cell. Because the thermal link between the sample cell and mixing chamber is weak, it takes more than 20 h to grow a solid sample, over which time considerable annealing takes place. Thus, as might be expected, we have found additional annealing of samples to have no effect on the measured heat capacity.

In Fig. 1 we show the heat capacity of the empty cell and solid ^{4}He samples with $x_3 = 1$ p.p.b., 0.3 p.p.m., 10 p.p.m. and 30 p.p.m. The contribution of the empty cell, which is one-tenth that of the solid helium over the entire temperature range, has been subtracted from the data. The departure from a T^3 dependence above 500 mK has been observed previously[12–16]. (See Supplementary Discussion for further details.) The most striking finding of this study is the excess heat capacity in addition to the Debye term at low temperature. It is nearly identical for the 1 p.p.b. and 0.3 p.p.m. samples, and becomes discernible below 140 mK. For the 10 p.p.m. and 30 p.p.m. samples the excess term is much larger and shows up below 200 and 250 mK, respectively.

It has been suggested that the observed NCRI is the consequence of solid helium's forming a glassy state and/or the inclusion of glassy regions in the sample[8,9,19,20]. A specific heat that is linear in T is a characteristic of glasses. In an attempt to extract such a linear term, in Fig. 2 we have plotted the temperature dependence of the specific heat C_n (per mole of ^{4}He), divided by T. If, in addition to the T^3 term, there is a component that scales linearly with T, the data will lie on a straight line with a non-zero y intercept. The data for $x_3 = 1$ p.p.b. and 0.3 p.p.m. between 140 and 430 mK do yield straight lines, but both lines extrapolate exactly through the origin, indicating that the specific heat above 140 mK is purely T^3. For comparison, the linear term in the specific heat deduced from recent pressure measurements[20] between 100 and 500 mK has a value of

$\sim$3 mJ mol^{-1} K^{-2}. This term was found to decrease by an order of magnitude after annealing of the solid sample. Given the scatter in the pressure data[20], the reduced value is indistinguishable from zero. We also searched for, but failed to find, any hysteresis or time-dependent effects characteristic of a glassy system. These results suggest that the glassy state is not present in solid samples that are cooled gradually or that have been annealed.

The data in Fig. 2 for the 10 p.p.m. and 30 p.p.m. samples do not fall on straight lines. Instead, the data seem to diverge in the low-temperature limit. This behaviour, which is more prominent in the 30 p.p.m. sample, suggests the presence of a temperature-independent term in addition to the Debye contribution. To test this idea, we plot C_n against T^3 in Fig. 3. In view of Fig. 2, it is not surprising that the data for $x_3 = 1$ p.p.b. and 0.3 p.p.m. fall on a straight line passing through the origin. The fact that the data for the 10 p.p.m. and 30 p.p.m. samples also fall on straight lines with non-zero intercepts confirms our conjecture of a constant term in the specific heat. When we fit each data set in the range 140 mK $< T <$ 430 mK, we obtain Debye temperatures (in K) of $\Theta = 29.1$, 27.6, 29.6 and 29.5 for the 1 p.p.b., 0.3 p.p.m., 10 p.p.m. and 30 p.p.m. samples, respectively. These values are within 10% of the expected values at similar pressures ($\sim$33 bar), with the main uncertainty coming from the absolute measurement of density. There is no *in situ* pressure gauge on the sample cell, but the initial pressure P_i and temperature T_i of the liquid before the formation of the solid block, as well as the approximate freezing point (breakaway point from the melting curve), are known. The densities deduced from P_i and T_i (0.192 ± 0.01 g cm^{-3}) are consistent with the observed freezing temperatures ($\sim 1.8 \pm 0.1$ K, corresponding to 0.194 ± 0.02 g cm^{-3}). The constant terms from the fit for $x_3 = 10$ p.p.m. and 30 p.p.m. are 59 ± 10 and 430 ± 40 μJ mol^{-1} K^{-1}, respectively. The y intercepts for the 1 p.p.b. and 0.3 p.p.m. samples, as shown in the inset to Fig. 3, are indistinguishable from zero; that is, they are within ± 5 μJ mol^{-1} K^{-1}. The slope (and thus Θ) and intercept from each fit change insignificantly if all the data below 430 mK are included in the analysis. The likely origin of the constant term is the presence of the ^{3}He impurities in the solid, which for $x_3 = 10$ p.p.m. and 30 p.p.m. correspond to $0.7 \pm 0.2 k_B$ and $1.7 \pm 0.3 k_B$ (where k_B is
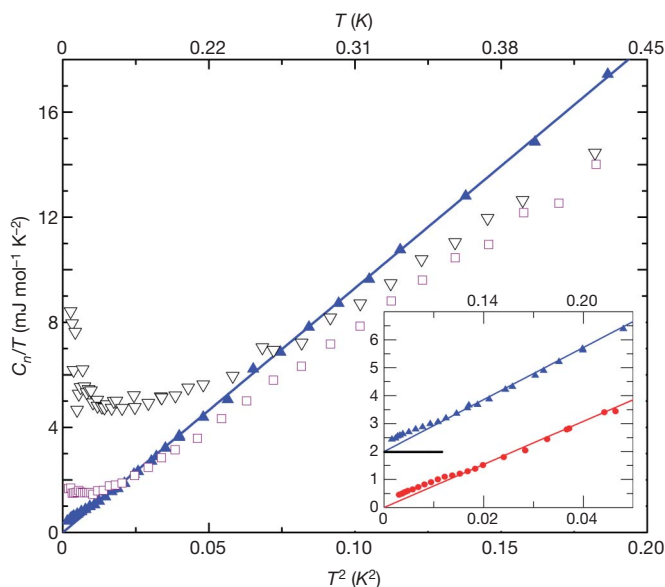
Figure 2 | Plot of C_n/T against T^2 for $x_3 = 1$ p.p.b., 0.3 p.p.m., 10 p.p.m. and 30 p.p.m. Black open triangles, 30 p.p.m.; purple open squares, 10 p.p.m.; blue triangles, 0.3 p.p.m.; red circles, 1 p.p.b. For clarity, the 1 p.p.b. data set is shown only in the inset. The blue line is the linear fit to the 0.3 p.p.m. data in the range 140 mK $< T <$ 430 mK. Inset, demonstration that the deviation from T^3 seen in the 1 p.p.b. and 0.3 p.p.m. samples exists only below 140 mK. In the inset the 0.3 p.p.m. data have been shifted upwards by 2 mJ mol^{-1} K^{-2}.
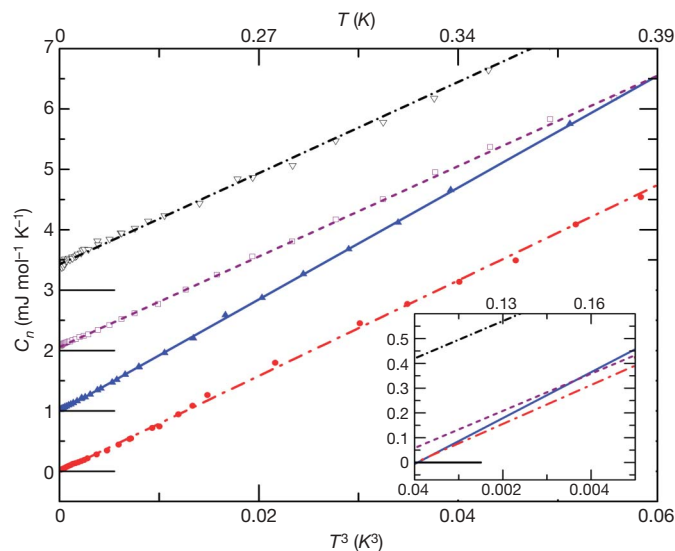
Figure 3 | Plot of specific heat against T^3. Data for the 0.3 p.p.m. (blue triangles), 10 p.p.m. (purple open squares) and 30 p.p.m. (black open triangles) samples have been shifted upwards by 1, 2 and 3 mJ mol^{-1} K^{-1}, respectively. The straight lines are linear fits of C_n versus T^3 between 140 mK and 430 mK. The deviation below 140 mK seen in the 1 p.p.b. (red circles) and 0.3 p.p.m. samples does not significantly affect the straight-line fit. Inset, fits without data points to demonstrate the zero intercepts for $x_3 = 1$ p.p.b. and 0.3 p.p.m. and the non-zero values for $x_3 = 10$ p.p.m. and 30 p.p.m.

the Boltzmann constant) per ^{3}He atom, respectively. There may also be a constant specific heat of the same order (per ^{3}He atom) for the 0.3 p.p.m. and 1 p.p.b. samples but it is undetectable given the small x_3.

NMR measurements[21–23] of dilute ^{3}He in solid ^{4}He have found that below 1.5 K the spin diffusion coefficient D increases with decreasing temperature, until it becomes independent of temperature below 0.8 K. For 100 p.p.m. $< x_3 <$ 500 p.p.m., and between 0.5 and 0.8 K, the diffusion coefficient satisfies[23] the relation $Dx_3 = 2.8 \times 10^{-11}$ cm^2. It is reasonable to assume that D continues to increase for even lower x_3. This behaviour has been interpreted in terms of an impuriton model in which ^{3}He impurities propagate coherently at low temperature as a wavelike excitation[21]. The constant specific heat found in the 10 p.p.m. and 30 p.p.m. samples is probably related to the high mobility of the ^{3}He impurities. (See Supplementary Discussion and Supplementary Fig. 1 for further details on ^{3}He impurities.) It is interesting that the magnitude ($\sim$1 k_B per ^{3}He atom) of the temperature-independent specific heat for $x_3 = 10$ p.p.m. and 30 p.p.m. is on the same order as that of a classical gas. The Fermi degeneracy temperatures of the 10 p.p.m. and 30 p.p.m. samples are 3 mK and 6 mK, respectively, well below the minimum temperature of the experiment.

When the T^3 phonon contribution is subtracted, a broad peak in the specific heat, C_{peak}, centred near 75 mK, is found for the 1 p.p.b., 0.3 p.p.m. and 10 p.p.m. samples. This is shown in the inset to Fig. 4. The peak for the 10 p.p.m. sample rides on top of the constant term of 59 μJ mol^{-1} K^{-1} deduced from Fig. 3. The main panel of Fig. 4 shows the peak with this constant term subtracted, together with those of the 1 p.p.b. and 0.3 p.p.m. samples. The data at high temperature ($T > 150$ mK) have larger scatter because the uncertainty scales with the total measured heat capacity. For the same reason the possible peak is indiscernible for $x_3 = 30$ p.p.m. The peak height in all three samples shown in Fig. 4 is $\sim$20 μJ mol^{-1} K^{-1} ($\sim$2.5 $\times 10^{-6}$ k_B per ^{4}He atom). The peak cannot be related to phase separation of the ^{3}He-^{4}He mixtures[17,24,25], in that it is not hysteretic and its magnitude is completely insensitive to a variation in x_3 of four orders of magnitude. (See Supplementary Discussion for a more detailed discussion on phase separation.) If we assume the specific heat extrapolates

linearly to zero at $T = 0$ K, the additional entropy associated with the peak increases from zero to about 28 μJ mol^{-1} K^{-1} (3.5×10^{-6} k_B per ^{4}He atom) as the temperature is raised from 0 K to 140 mK.

The melting curve of pure ^{4}He was recently measured[26,27] at high resolution between 10 and 320 mK. After the data below 80 mK had been adjusted for an instrumental effect[27], the melting curve followed a T^4 dependence with an uncertainty of about 1 μbar. This implies a T^3 specific heat for both the solid and liquid phases. If we assume that solid in coexistence with liquid is thermodynamically identical to that near 33 bar, the additional contribution to the pressure that stems from the peak in Fig. 4 would cause a deviation of about 5 μbar in a T^4 power-law fit of the melting curve. We do not have an explanation for this apparent discrepancy.

As noted above, the onset of NCRI in 1 p.p.b. solid helium samples is 75 mK (ref. 10). There is evidence that the higher T_o values found in 0.3 p.p.m.[1–6,8,10] samples and at larger concentrations (E. Kim, J. S. Xia, J. T. West, X.L. and M.H.W.C., unpublished observations) are due to a finite vortex response time[6,11], and that the 'true' transition temperature in the zero frequency limit may also be near 75 mK, independently of ^{3}He concentration. A systematic study of the frequency dependence of NCRI in samples of different x_3 will be needed to test this speculation. Nevertheless, the coincident peak in heat capacity and onset of NCRI in 1 p.p.b. samples make it probable that we have observed the thermodynamic signature related to NCRI. The temperature dependence of NCRI in 1 p.p.b. samples[10] may be consistent with a transition that falls into the same universality class as the lambda transition in liquid ^{4}He. If this is indeed so, NCRIF can be calculated by means of the two-scale-factor universality hypothesis. This prediction has been tested and found satisfactory for the superfluid transition of liquid ^{4}He under pressure[28] and for liquid helium confined in porous media[29,30]. If we use the peak height as the amplitude of the singular specific heat then, when compared with the superfluid transition, the NCRIF should be 0.06%. This number lies between 0.03% (E. Kim, J. S. Xia, J. T. West, X.L. and M.H.W.C., unpublished observations) and 0.3% (ref. 10), which are the fractions observed in torsional oscillator studies of 1 p.p.b. samples. This comparison indicates the magnitude of the specific heat peak is at least not unphysical.

Thus, our measurements of specific heat in solid ^{4}He with 10 p.p.m. and 30 p.p.m. ^{3}He found evidence of a constant-specific-heat term that scales with ^{3}He concentration. This term is probably related to the high, temperature-independent, mobility of dilute ^{3}He impurities found in NMR studies. We also found a broad peak in specific heat centred near 75 mK in 1 p.p.b., 0.3 p.p.m. and 10 p.p.m. samples. This peak is very likely to be the thermodynamic signature of the supersolid phase.
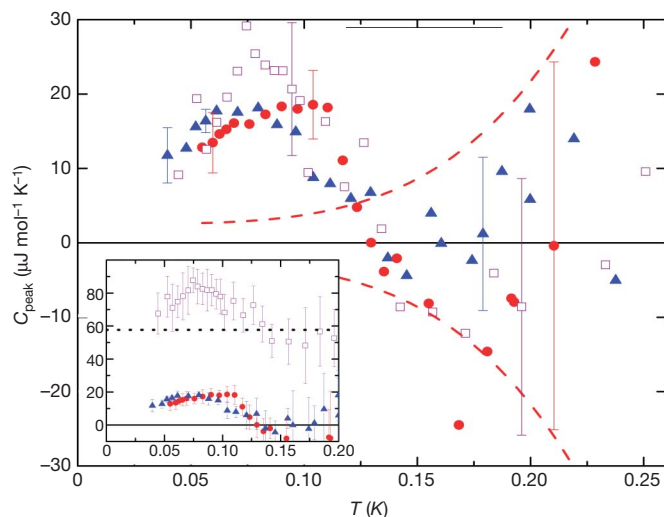
Figure 4 | Specific heat peaks of the 1 p.p.b., 0.3 p.p.m. and 10 p.p.m. samples. Purple open squares, 10 p.p.m.; blue triangles, 0.3 p.p.m.; red circles, 1 p.p.b. The x_3-independent peak centred near 75 mK is revealed when the phonon contribution is subtracted. The s.d. of the 1 p.p.b. data set is shown as red dashed lines. The s.d. for $x_3 = 0.3$ p.p.m. is comparable. For $x_3 = 10$ p.p.m., it is similar above 200 mK but decreases more gradually with decreasing temperature. Inset, comparison of the specific heat of the three samples before subtraction of the constant term of the 10 p.p.m. sample (dotted line at 59 μJ mol^{-1} K^{-1}).

1. Kim, E. & Chan, M. H. W. Probable observation of a supersolid helium phase. *Nature* **427**, 225–227 (2004).
2. Kim, E. & Chan, M. H. W. Observation of superflow in solid helium. *Science* **305**, 1941–1944 (2004).
3. Rittner, A. S. C. & Reppy, J. D. Observation of classical rotational inertia and nonclassical supersolid signals in solid ^{4}He below 250 mK. *Phys. Rev. Lett.* **97**, 165301 (2006).
4. Kondo, M., Takada, S., Shibayama, Y. & Shirahama, K. Observation of non-classical rotational inertia in bulk solid ^{4}He. *J. Low Temp. Phys.* **148**, 695–699 (2007).
5. Penzev, A., Yasuta, Y. & Kubota, M. Annealing effect for supersolid fraction in ^{4}He. *J. Low Temp. Phys.* **148**, 677–681 (2007).
6. Aoki, Y., Graves, J. C. & Kojima, H. Oscillation frequency dependence of nonclassical rotation inertia of solid ^{4}He. *Phys. Rev. Lett.* **99**, 015301 (2007).
7. Leggett, A. J. Can a solid be 'superfluid'? *Phys. Rev. Lett.* **25**, 1543–1546 (1970).
8. Rittner, A. S. C. & Reppy, J. D. Disorder and the supersolid state of solid ^{4}He. *Phys. Rev. Lett.* **98**, 175302 (2007).
9. Prokof'ev, N. V. What makes a crystal supersolid? *Adv. Phys.* **56**, 381–402 (2007).
10. Clark, A. C., West, J. T. & Chan, M. H. W. Nonclassical rotational inertia in helium crystal. *Phys. Rev. Lett.* **99**, 135302 (2007).
11. Anderson, P. W. Two new vortex liquids. *Nature Phys.* **3**, 160–162 (2007).
12. Heltemes, E. C. & Swenson, C. A. Heat capacity of solid ^{3}He. *Phys. Rev.* **128**, 1512–1519 (1962).

13. Edwards, D. O. & Pandorf, R. C. Heat capacity and other properties of hexagonal close-packed helium-4. *Phys. Rev.* **140**, A816–A825 (1965).

14. Gardner, W. R., Hoffer, J. K. & Phillips, N. E. Thermodynamic properties of ^{4}He. The hcp phase at low densities. *Phys. Rev. A.* **7**, 1029–1043 (1973).

15. Castles, S. H. & Adams, E. D. Specific heat of solid helium. *J. Low Temp. Phys.* **19**, 397–431 (1975).

16. Hébral, B., Frossati, G., Godfrin, H., Thoulouze, D., Greenberg, A. S. & in. *Phonons in Condensed Matter* (ed. Maris, H. J.) 169–172 (Plenum, New York, 1980).

17. Clark, A. C. & Chan, M. H. W. Specific heat of solid helium. *J. Low Temp. Phys.* **138**, 853–858 (2005).

18. Sullivan, P. F. & Seidel, G. Steady-state, ac-temperature calorimetry. *Phys. Rev.* **173**, 679–685 (1968).

19. Nussinov, Z., Balatsky, A. V., Graf, M. J. & Trugman, S. A. Origin of the decrease in the torsional-oscillator period of solid ^{4}He. *Phys. Rev. B* **76**, 014530 (2007).

20. Grigorev, V. N. *et al.* Observation of a glassy phase in solid ^{4}He in the supersolidity region. Preprint at 〈http://arxiv.org/abs/cond-mat/0702133〉 (2007).

21. Richards, M. G., Pope, J. & Widom, A. Evidence for isotopic impuritons in solid helium. *Phys. Rev. Lett.* **29**, 708–711 (1972).

22. Grigor'ev, V. N. *et al.* ^{3}He impurity excitations in solid ^{4}He. *J. Low Temp. Phys.* **13**, 65–79 (1973).

23. Allen, A. R., Richards, M. G. & Schratter, J. Anomalous temperature dependence of D and T_2 for dilute solutions of ^{3}He in solid ^{4}He. *J. Low Temp. Phys.* **47**, 289–320 (1982).

24. Hébral, B. *et al.* Fermi-liquid droplets in liquid-solid solutions of the helium isotopes. *Phys. Rev. Lett.* **46**, 42–45 (1981).

25. Schrenk, R., Friz, O., Fujii, Y., Syskakis, E. & Pobell, F. Heat capacity and pressure at phase separation and solidification of ^{3}He in hcp ^{4}He. *J. Low Temp. Phys.* **84**, 133–156 (1991).

26. Todoshchenko, I. A. *et al.* Melting curve of ^{4}He: no sign of a supersolid transition down to 10 mK. *Phys. Rev. Lett.* **97**, 165302 (2006).

27. Todoshchenko, I. A., Alles, H., Junes, H. J., Parshin, A., Ya. & Tsepelin, V. Absence of low temperature anomaly on the melting curve of ^{4}He. *JETP Lett.* **85**, 555–558 (2007).

28. Singsaas, A. & Ahlers, G. Universality of static properties near the superfluid transition in ^{4}He. *Phys. Rev. B* **30**, 5103–5115 (1984).

29. Yoon, J. & Chan, M. H. W. Superfluid transition of ^{4}He in porous gold. *Phys. Rev. Lett.* **78**, 4801–4804 (1997).

30. Zassenhaus, G. M. & Reppy, J. D. Lambda point in the ^{4}He-Vycor system: a test of hyperuniversality. *Phys. Rev. Lett.* **83**, 4800–4803 (1999).

Author Contributions X.L., A.C.C. and M.H.W.C. contributed equally to this work.

Author Information Reprints and permissions information is available at www.nature.com/reprints. Correspondence and requests for materials should be addressed to M.H.W.C. (chan@phys.psu.edu).